

High unimer concentration and asymmetric bilayer observed in small unilamellar vesicles of mixed surfactants TDMAO/LiPFO

Anja F. Hörmann,¹ Artem Feoktystov,² Theyencheri Narayanan,³ Jeremie Gummel,³ and Michael Gradzielski¹

¹*Stranski-Laboratorium für Physikalische und Theoretische Chemie, Institut für Chemie, Technische Universität Berlin, D-10623 Berlin, Germany*

²*Forschungszentrum Jülich GmbH, Jülich Centre for Neutron Science (JCNS) at Heinz Maier-Leibnitz Zentrum, D-85748 Garching, Germany*

³*European Synchrotron Radiation Facility, 71 avenue des Martyrs, F-38043 Grenoble Cedex 9, France*

(*Electronic mail: a.hoermann@tu-berlin.de)

(Dated: 12 May 2023)

The mixed surfactant system tetradecyldimethylamine oxide (TDMAO) and lithium perfluorooctanoate (LiPFO) is known to spontaneously self-assemble into well-defined small unilamellar vesicles (SUVs). For a quantitative analysis of Small-Angle X-ray Scattering (SAXS) on this model system, we complemented the measurements with densitometry, conductimetry, and contrast-variation Small-Angle Neutron Scattering (SANS). The analysis points to two main findings: first, the vesicles formed contain a much higher mole fraction (0.61-0.64) of TDMAO than the bulk sample (0.43) and predicted by Regular Solution Theory (RST, 0.46). In consequence, the unimer concentration of LiPFO is more than 5 times higher than predicted by RST. Second, the vesicle bilayer is asymmetric with a higher fraction of LiPFO on the outside. These findings on a model system should be of broader relevance for the understanding of similar mixed surfactant vesicle systems and thereby also be of importance for their use in a number of applications.

I. INTRODUCTION

The study of self-assembled small unilamellar vesicles (SUVs, see e.g. the reviews by Gradzielski¹ and Šegota et al.² for an overview) is of relevance for the development of applications like encapsulation of active agents and ultimately drug delivery³. In order to control vesiculation for this purpose, it is important to understand both the self-assembly process and its final state. For the case of surfactant mixtures, e.g., catanionic ones, several studies on the formation pathway have shown that it proceeds via disk-like micelles as intermediate structures.^{4–8}. Here, the interplay of bending rigidity and line tension of the bilayer⁹ governs the transition from disk-like micelles to vesicular aggregates, whose structure then is kinetically controlled. A model system showing spontaneous vesiculation¹⁰ within a time range observable with stopped-flow SAXS^{11,12} consists of a short-chain anionic perfluorinated surfactant mixed with a zwitterionic C₁₄-chain surfactant. In that context it might be noted that mixtures of perfluorinated and normal hydrocarbon surfactants have been studied to quite an extent before. In general, it is observed that antagonistic interactions exist between them due to the unfavorable interactions between the hydrocarbon and perfluoro chains. Nonetheless, one observes formation of mixed micellar aggregates, as for instance verified by small-angle neutron scattering (SANS) experiments on ammonium decanoate and ammonium perfluoro-octanoate (APFO). The mixed micelles are larger than the homomicelles and the mixed micelles were found to contain more APFO than expected for ideal mixing¹³.

Previous studies have shown that the mechanism of vesicle formation in this system occurs via a disk-like or torus-like structure, depending on concentration¹⁴. The kinetics of this transformation from disk-like mixed micelles to vesicles and the resulting vesicles size are determined by the competing contributions of line tension and bending energy to the free energy^{6–8,15–17} and the process could be controlled by the addition of amphiphilic copolymers¹⁶. Kinetic aspects of these model systems are therefore well-known, there are still open questions regarding the detailed structure and composition of the formed vesicles as well as the thermodynamic conditions prevailing within in the bilayer.

The chosen surfactant mixture is a model system, where the use of a perfluorinated surfactant allows a detailed investigation of the relative location of the individual surfactants within a bilayer. Such structural details are typically difficult to see in fully hydrogenated surfactant mixtures. Moreover, the system chosen here exhibits good scattering contrast between their two

component molecules for both x-ray and neutron scattering¹⁸, and therefore is very well-suited to address questions like the internal structure of the bilayer, for example, the question if the distribution of molecules is symmetric or asymmetric, as well as how its composition is related to the bulk composition of the mixture. The mixing ratio of TDMAO/LiPFO was selected such to deliver very well-defined vesicles¹⁵. The observed relatively large deviation from a simple expectation is interesting as it should be relevant for other anionic-zwitterionic systems where similarly more complex situations might be present.

II. MATERIALS AND METHODS

A. Materials

Tetradecyldimethylammonium oxide (TDMAO, $C_{14}H_{29}(CH_3)_2NO$) was received free of charge from Stepan (Stepan Company, Northfield, Illinois, USA) as Ammonyx M solution, freeze dried and used without further purification. Lithium perfluorooctanoate (LiPFO) was obtained by neutralization of perfluorooctanoic acid ($C_7F_{15}COOH$, Sigma-Aldrich, > 96%) using lithium hydroxide (LiOH, Fluka, $\geq 99.5\%$) solution. Pluronic L35 ($EO_{11}PO_{16}EO_{11}$) was obtained free of charge from BASF (BASF SE, Ludwigshafen am Rhein, Germany) and used without further purification. H_2O from a Millipore water filter and D_2O (deutero, 99.9%) were filtrated with a $0.45\ \mu m$ regenerated cellulose filter.

1. Sample Preparation

Samples were prepared by mixing solutions of TDMAO and LiPFO stock solutions at the same concentration, 25 mM in most cases, in the appropriate ratio to obtain a specific mole fraction of TDMAO in the sample α_T . We used adjustable pipettes for rapid mixing and a well-defined sample age, and noted the weights of both solutions.

For the contrast-variation Small-Angle Neutron Scattering (SANS) experiment, stock solutions of both TDMAO and LiPFO in light and heavy water were mixed to adjust the volume fraction of D_2O before mixing the two surfactants, such that the mixture was always formed in the last step. Furthermore, the TDMAO stock solutions contained 0.5 mol% of Pluronic L35 with respect to TDMAO for suppressing ageing effects, an addition which later proved to have negligible effect.

B. Experimental Methods

1. Densitometry

Density of TDMAO, LiPFO and TDMAO/LiPFO mixtures at $\alpha_T = 0.3, 0.4, 0.5, 0.6$ and 0.7 was determined using an Anton-Paar DMA 4500 instrument at $25.00(2)^\circ\text{C}$. Assuming additivity of volumes, the effective density of the surfactants at each mixing ratio was determined using a dilution series of five points each in the vesicle forming region. The resulting molecular volumes and scattering length densities are summarized in the Supporting Information (SI, section SI).

2. Conductometry

Conductivity measurements were carried out using a Mettler Toledo SevenCompact conductometer equipped with an InLab 752-6 mm electrode. We employed the built-in nonlinear Automatic Temperature Correction (ATC) to correct for small deviations in temperature from 25.0°C up to 0.4°C as per specifications.

Concentration dependent conductivity of LiPFO in H_2O was recorded using a thermostated container attached to a Metrohm Titrando apparatus which was used to control temperature at 24.7°C and add water in a controlled fashion. The concentration series was prepared by stepwise dilution of a 45 mM solution. After each addition of water the solution temperature was allowed to equilibrate and the conductivity was constant for at least 20 s before each measurement, the upper limit of the response time of the electrode as per its specifications.

The conductivity of the TDMAO/LiPFO mixture with $43\text{ mol}\%$ TDMAO was measured for two samples in H_2O previously prepared for light scattering measurements and stored at room temperature. Samples were allowed to equilibrate at 25.0°C for 30 min before the measurement and conductivity recorded as described for LiPFO.

A concentration series of vesicle-forming samples of the same mixing ratio $\alpha_T = \frac{3}{7}$ was prepared in H_2O by dilution of a sample at 50 mM total surfactant concentration to 4 mM , 8 mM , 12.5 mM , 25 mM and 37.5 mM . Samples were stored in a water bath at $25.5(5)^\circ\text{C}$ and vortexed twice a week for 14 days . Measurements were performed 14 days after mixing at $25.0(1)^\circ\text{C}$.

3. Light Scattering

Static and dynamic light scattering were measured simultaneously on an ALV-CGS3 instrument ($\lambda = 632.8\text{ nm}$) at 25.0°C . Quartz cuvettes (8 mm diameter) were used as sample containers.

For measurements of equilibrated samples of different concentrations (details of preparation: see II B 2; filtration was limited to the solvent to exclude any effects on the sample) three 30 s measurements per angle were carried out from 20° to 150° in 5° steps.

Data were corrected by subtracting solvent and normalising with respect to toluene:

$$I(q) = \frac{\frac{CR}{\text{monitor}}|_{\text{sample}} - \frac{CR}{\text{monitor}}|_{\text{solvent}}}{\frac{CR}{\text{monitor}}|_{\text{toluene}}} \cdot R_{\text{toluene}}$$

where $R_{\text{toluene}} = 1.34 \times 10^{-5} \text{ cm}^{-1}$.

4. X-ray Scattering

Samples used for the SAXS/WAXS measurements were relatively fresh, prepared on the day of the measurements. Small-angle X-ray scattering (SAXS) and wide-angle X-ray scattering (WAXS) measurements were carried out at ID02, ESRF (Grenoble, France) employing a wavelength of 0.1 nm at a sample-to-detector distance of 2.5 m for SAXS and 0.12 m for WAXS. Two-dimensional SAXS/WAXS patterns were simultaneously recorded using a FReLoN 4M CCD detector for SAXS and an AVIEX PCCD detector for WAXS. Measured scattering patterns were corrected for the dark current, spatial inhomogeneities and normalized to an absolute scale. The one-dimensional SAXS/WAXS profiles were obtained by the azimuthal averaging of the isotropic two-dimensional patterns. To avoid radiation damage, multiple 5 ms detector frames were taken, which were subsequently averaged. To ensure accurate background subtraction, all SAXS/WAXS measurements were carried out using a flow-through capillary cell. The background scattering was measured with the flow-through capillary filled with water and normalized as in the case of the samples. Scattering vector resolution was $\sigma_q = 4 \times 10^{-3} \text{ nm}^{-1}$ and taken into account via a pinhole resolution function. For analysis, we chose to weigh all datapoints equally, using $\Delta y = y_{\text{theory}} - y_{\text{data}}$ as residuals, where y was either I or Iq^2 .

5. *Small-Angle Neutron Scattering (SANS)*

All samples were prepared from individual surfactant solutions a few hours before measurements and within five minutes of each other. Due to limited precision of the adjustable pipettes employed the volume fraction of surfactant was ϕ (0.00613(7)) and mixing ratio α_T (0.3941 to 0.438). SANS was measured at three configurations (sample-to-detector distance = 1.19 m, 7.69 m and 19.69 m) using neutrons of wavelength $\lambda = 5 \text{ \AA}$ at KWS-1, FRM II (Garching, Germany). These configurations were measured from high to low q and the sample age for each sample and configuration is shown in table SIII.

Background subtraction, transmission correction and radial averaging were done in QtiKWS¹⁹. The resulting scattering vector q and its standard deviation σ_q as well as scattering intensity I and its standard deviation σ_I were employed for the analysis.

C. Theory

1. *Regular Solution Theory*

Regular solution theory (RST) is a thermodynamic description for binary surfactant mixtures based on a pseudophase separation approach²⁰. It allows for non-ideal mixing behavior of the two surfactants described by the interaction parameter $\beta = \frac{1}{k_B T} (W_{11} + W_{22} - 2W_{12})$. Nonideality ($\beta \neq 0$) arises if inter-species interactions W_{12} are more (or less) favourable than the average intra-species interaction energy W_{ii} . The activity coefficients f_i for each species i in the micelle are assumed to be $f_i = \exp(\beta(1 - x_i)^2)$, $i \in [1, 2]$, with x_i the mole fraction in the aggregate. Hence, thermodynamic potentials are symmetrical with respect to $x_i = 0.5$.

According to Holland and Rubingh²¹, the equilibrium in a non-ideal binary surfactant mixture at the mixed cmc is given by:

$$\frac{(x_1)^2 \ln \left(\frac{\alpha_1 \text{cmc}_{12}}{x_1 \text{cmc}_1} \right)}{(1 - x_1)^2 \ln \left[\frac{(1 - \alpha_1) \text{cmc}_{12}}{(1 - x_1) \text{cmc}_2} \right]} = 1 \quad (1)$$

$$\frac{\ln \left(\frac{\alpha_1 \text{cmc}_{12}}{x_1 \text{cmc}_1} \right)}{(1 - x_1)^2} = \beta \quad (2)$$

with the mole fraction of surfactant 1 in the sample α_1 , the mole fraction of surfactant 1 in the aggregate x_1 as well as the individual critical micellization concentrations cmc_i and the crit-

ical aggregation concentration at composition α_1 , cmc_{12} . At higher concentrations, this can be generalized to (Rubingh²⁰, eq. 14):

$$x_1 = \frac{-(c_{\text{tot}} - \Delta) + \sqrt{(c_{\text{tot}} - \Delta)^2 + 4 \cdot \Delta \cdot c_{\text{tot}} \cdot \alpha_1}}{2 \cdot \Delta} \quad (3)$$

$$\Delta = \text{cmc}_2 \cdot f_2(x_1, \beta) - \text{cmc}_1 \cdot f_1(x_1, \beta) \quad (4)$$

This equation is solved numerically to predict the fraction of surfactant 1 in the aggregate x_1 at total surfactant concentration c_{tot} . The predicted unimer concentrations are then calculated using conservation of concentrations (Rubingh²⁰, eq. 9):

$$\frac{\alpha_1 c_{\text{tot}}}{c_{\text{tot}} + f_1 \cdot \text{cmc}_1 - M} + \frac{(1 - \alpha_1) c_{\text{tot}}}{c_{\text{tot}} + f_2 \cdot \text{cmc}_2 - M} = 1 \quad (5)$$

$$\text{with } M = c_1^{\text{uni}} + c_2^{\text{uni}} \quad \text{and} \quad c_1^{\text{uni}} = \frac{M - f_2 \text{cmc}_2}{1 - \frac{f_2 \text{cmc}_2}{f_1 \text{cmc}_1}} \quad (6)$$

Predictions for a range of c_{tot} and β can be found in the SI (Fig. S16). Regular Solution Theory has been applied to spontaneously formed vesicles in a number of studies^{15,22,23}.

D. Numerical Methods

1-dimensional small-angle scattering data were analyzed using Markov-Chain Monte Carlo (MCMC) sampling of the parameter space in the case of homogeneous shell models. We employed χ^2 as the negative log-likelihood, assuming uncertainties follow a Gaussian distribution. For this purpose, we used the DREAM algorithm²⁴ as implemented in the Python package bumps (0.9.0)²⁵ together with customized SasView (5.0.4) models. Source code is available as electronic supporting information²⁶.

III. RESULTS

A. Basic Structural Features: SAXS

Using classical methods to analyze SAS data we obtain first estimates on the nanostructure of our samples. From low to high q , we observe a plateau, 3-4 pronounced local minima ("oscillations") and a minimum followed by a broad maximum (see Fig. 1). In the WAXS region the intensity decreases and there is a peak at 13.3 nm^{-1} corresponding to the packing of disordered surfactant chains.

From the shape of the scattering curve with a q^{-2} intensity decrease and the local minima (Fig. 1), whose position increases linearly with their number, one can conclude the presence of vesicles. The radius of the corresponding infinitely thin hollow sphere in agreement with $q_{\min,n}R = n\pi$ is about 10.68(3) nm (Fig. 1 c), and thereby in good agreement with the radius of gyration 9.73(19) nm (see Fig. 1 a).

For hollow spheres, we expect a second (series) of minima corresponding to the thickness at high q , where the first minimum is seen around 1.2 nm^{-1} . Intensity increases again afterwards and forms a broad maximum around 2.3 nm^{-1} (Fig. 1 a). Local minima from the thickness of a homogeneous hollow shell ($R = 9.39(22) \text{ nm}$, $d = 3.97(9) \text{ nm}$) would appear at much lower intensities, indicating an internal structure with a repeating distance of $\approx 2.7 \text{ nm}$.

By comparison with reference data on LiPFO and TDMAO solutions in the concentration range of interest (Fig. S2), we observe a similarity between scattering from LiPFO unimers and our sample in the range $3 \text{ nm}^{-1} \leq q \leq 8 \text{ nm}^{-1}$. The decrease approximately follows q^{-1} in both cases which hints at elongated structures.

Finally, the small WAXS peak at about 13.3 nm^{-1} (see Fig. 1 a) is likely due to liquid-like surfactant chain packing¹⁸.

TABLE I. Models shown in Fig. 1.

model	I_0 / cm^{-1}	radius / nm	comment
Guinier	2.81(3)	9.73(19)	$qR \leq 1.16(2)$
thin shell	2.81(3)	10.68(3)	
hollow sphere	2.81(3)	9.39(22)	$d = 3.97(9) \text{ nm}$

B. Vesicle Composition and Free LiPFO

I. SAXS

A more detailed analysis of the SAXS data with a homogeneous spherical shell to model our SUVs yields the forward scattering intensity $I_0 \approx 2.81(3) \text{ cm}^{-1}$ and an approximate mean radius of the vesicles $R \approx 10.0 \text{ nm}$.

Using previous findings on the thermodynamics of the system by Wolf et al.¹⁰, we can further calculate the expected composition of the vesicular aggregates $x \approx 0.46$ as well as the concen-

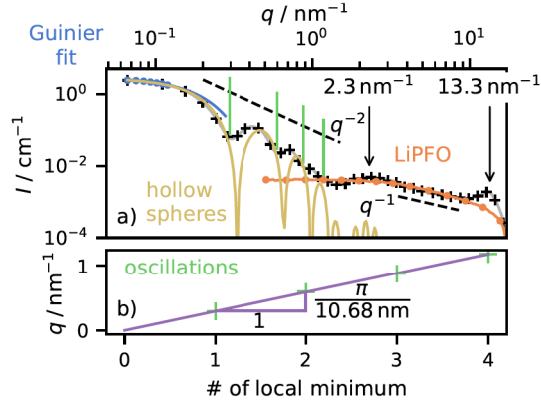


FIG. 1. a) First quantitative description of the data (gray line; every fifth point marked by black +) using the Guinier approximation at low q and the positions of the local minima. The positions of the local minima (green vertical lines) were determined using a peak-finding algorithm (see Fig. S3 b). The radius of gyration was obtained from a fit of the Guinier approximation $I(q) = I_0 \exp(-R_g^2/3 \times q^2)$ to the filled datapoints. The bilayer thickness was estimated using a modified Guinier plot for flat objects (Eq. S1, Fig. S3 a). For the hollow sphere form factor the radius was calculated such that $R_g = 9.73(19)$ nm. b) The local minima follow the law $q = \frac{n \cdot \pi}{R}$ characteristic for hollow shells.

tration of free surfactant $c_{\text{unimers}} \approx 1.48$ mM (0.00193 mM TDMAO and 1.48 mM LiPFO, i.e. 94 mol% in aggregates) using regular solution theory (RST, see e.g.²⁰) and $\beta = -12$ for the interaction parameter (¹⁰, from cmc measurements). Together with I_0 and R , these parameters fully define the vesicle model ($\phi_{\text{vesicles}} = 5.86 \times 10^{-3}$, $\Delta\text{SLD} = 2.87 \times 10^{-4} \text{ nm}^{-2}$) and yield a thickness $d = 0.47$ nm, which is in marked disagreement with our expectations for such surfactant aggregates and in clear disagreement with the experimental data, where a much larger bilayer thickness is seen, as shown in Fig. 2.

As the forward scattering intensity is given as $I_0 = \phi V_{\text{ves}} \cdot \Delta\text{SLD}^2 = 2.81(3) \text{ cm}^{-1}$ and the vesicle radius is determined by the first minimum, the mismatch in thickness must arise from a lower volume fraction of vesicles ϕ since such major discrepancy cannot arise from uncertainties in the SLD (which is given via the density). In any way the scattering intensity is determined by the amount of dispersed scattering length and apparently this is substantially less than expected.

This means that effectively a much smaller fraction of the surfactant must be aggregated, where in particular the high contrast perfluorinated surfactant must be missing. This opens up two ques-

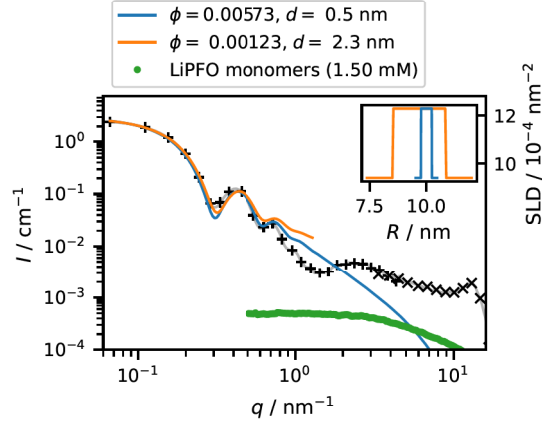


FIG. 2. Simulation of hollow shell scattering with the expected volume fraction (blue; thickness $d = 0.47$ nm from RST ($\beta = -12$) and I_0 , Schulz-Zimm distributed radius with mean 10 nm and 12 % polydispersity) and fitted volume fraction (orange; thickness, volume fraction and radius optimized against I). The fit leads to a lower ϕ and higher d . To illustrate the expected scattering from LiPFO unimers at the predicted concentration, we multiplied scattering data at 12.5 mM by the appropriate factor 0.12.

tions: 1. what is the precise composition of the vesicle bilayers? 2. why is it significantly deviating from the one predicted by RST?

2. Aggregate Composition: Contrast Variation SANS

To determine the mole fraction of both surfactants in our aggregates, we employed contrast-variation Small-Angle Neutron Scattering (SANS).

To stabilise the vesicles against ageing, amphiphilic copolymer of the Pluronic type (PEO-PPO-PEO) was added as previously used by Bressel et al.¹⁶ for TDMAO/LiPFOS (Lithium perfluorooctane sulfonate), which allows to control size and stability of the SUVs.

For that purpose our vesicles contain 0.5 mol % Pluronic L35 ($\text{EO}_{11}\text{PO}_{16}\text{EO}_{11}$) with respect to TDMAO. As shown in Fig. S8, the effect of L35 on our TDMAO/LiPFO sample is rather insignificant (leading to a size increase of 2.3 %), thereby being well-comparable to the samples without L35 used in SAXS.

The progression of the scattering curves $I(q)$ with the solvent composition (hence, SLD) is shown in Fig. 3. Data were analyzed using a vesicle form factor model where the mole fraction

of TDMAO in the vesicle x_T determines SLD and volume fraction under the assumption that TDMAO unimers are negligible. Simultaneous optimization included x_T , R and d as parameters, and details of the modelling are explained in the SI. Best-fit results are shown in Fig. 3 together with the probability density function (pdf) for x_T from MCMC sampling, which indicates a narrow range of credible values for this parameter. Distributions and correlations for all three parameters can be found in the supporting information S9.

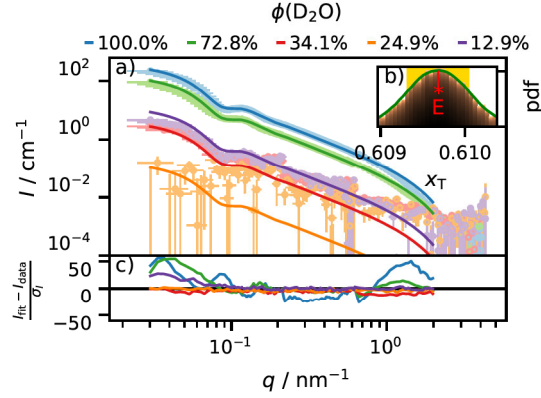


FIG. 3. Simultaneous optimization of x_T , R and d on SANS contrast variation data. a) Data and hollow spheres with the best-fit values for mole fraction of TDMAO $x_T = 0.61$. b) Probability density function of the variable x_T resulting from the DREAM optimization. The histogram shows the sum of $-\log p$ of points visited during MCMC sampling, whereas marginal likelihoods are represented by the green line. l, * and E represent the median, best and mean values of x_T c) Residuals.

The result is particularly obvious due to the large difference in SLD between both surfactants which is present in neutron scattering also (see table SI). Compared to the predicted $x_T = 0.46$ (see IIIB 1), this experimental mixing ratio increases contrast in SANS, but reduces it in SAXS.

3. Conductivity

Compared to RST predictions, the higher fraction of TDMAO in the SUVs found using SANS requires more LiPFO to be present as unimers. LiPFO micelles are not expected below the reported cmc, 33.4mM. Conductimetry was measured to check if data are consistent with these expectations and thereby also with our SAS analysis.

For calibration we measured the conductivity of the pure LiPFO solution as a function of concentration at 25.0 °C (figure S12 in the SI), these are comparable to values reported by Gianni et al.²⁷.

For the vesicle samples good agreement with the values of the pure LiPFO solutions is observed until a concentration of ≈ 8 mM is reached. Above that, sample conductivities are lower than those of the corresponding LiPFO solutions. Our measurements are in agreement with data reported by Wolf et al.¹⁰ at 50 mM total concentration, assuming Kohlrausch's law holds.

The observed reduced conductivity can be partially ascribed to entrapment effects due to the presence of vesicles and they were taken into account as specified in the supporting information SIV.

The other effect is counterion condensation θ (which is also the basis for cmc determination by conductivity experiments) on the outer surface of the vesicle is estimated using Manning theory for a plane wall (with $\kappa l_B \ll 1$, as $\kappa R_h \ll 1$ for the measured vesicle sizes) which yields²⁸:

$$1 - z\theta = -\frac{e_0 \kappa \ln(\kappa l_B)}{2\pi z l_B \sigma} \quad (7)$$

where $z = 1$ is the valence of the counterion (Li^+), κ the inverse Debye length, l_B the Bjerrum length and σ the unscreened charge density of the surface (without condensation). We find values around 0.8 for all samples assuming that 52 % of LiPFO is free and contributes to screening (see Fig. S15).

We can now estimate the contributions of vesicles, free counterions, and LiPFO unimers to the conductivity of the samples. First, the lithium ions: $\kappa = c \cdot \Lambda = c \cdot [\Lambda_0 - (0.230\Lambda_0 + 60.68)\sqrt{c/\text{mol/L}}]$. Second and similarly we estimate the PFO^- contribution using the measured $\Lambda_{\text{PFO}^-}^0 = 27.98 \text{ mS cm}^{-1} \text{ mol}^{-1} \text{ L}$ (see S13). Finally, the vesicles are treated as macroions with radius R_h contributing $\Lambda = \frac{Ze}{6\pi\eta R_h} \cdot ZF = \mu ZF$ with the Faraday constant F . The number of charges on the outside of one vesicle Z is calculated using θ , the mixing ratio of surfactants in the vesicle as well as the surface area ($4\pi R_h^2$).

Figure 4 shows the estimated conductivity of each of the contributing populations: ions, unimer, and vesicles. Calculations were performed assuming either a constant fraction of free LiPFO (dashed lines) or RST with an interaction parameter of -1 which predicts unimer concentrations and composition close to the observed ones at $c_{\text{tot}} = 25$ mM (solid lines, see S16). In both cases, conductivity is dominated by the lithium ions followed by the perfluorinated unimer. As expected, the vesicular contribution is negligible: while the specific conductivity ($3 \times 10^5 \text{ mS/cmL/mol}$

to 1×10^5 mS/cmL/mol) is higher than the values for ions and unimer, the molar concentration (mole vesicles per liter) is of the order of 4×10^{-9} mol/L to 1×10^{-7} mol/L, hence the product $\kappa = \Lambda c_{\text{ves}}$ is negligible.

Experimentally we find a higher conductivity, which could arise from a higher degree of Li^+ dissociation compared to predictions, but given the electrostatic conditions this is an unlikely scenario. To compensate for the discrepancy by either counterion or PFO^- release from the vesicle, several mM of either species would be needed, hence this is unlikely in both cases. Alternative explanations include too crude approximations in the conductivity models, a slight underestimation of $c(\text{PFO}^-)$ in SANS, and finally the cmc of LiPFO which may be 10% lower judging from the conductivity measurements as shown in the SI (Fig. S12).

The PFO^- concentrations used for Fig. 4 at 25 mM surfactant concentration are 8.13 mM (RST, $\beta = -1$) and 7.41 mM (constant x_T , 52% PFO^- unassociated). Looking at Fig. 4, the former is in better agreement with the qualitative trend of the experimental data and its quantitative values at the lower concentrations but the deviation between both models is small at 25 mM.

Overall, we have shown that conductivity measurements are consistent with LiPFO unimer concentrations much higher than the initially predicted 1.48 mM (RST, corresponds to $x_T = 0.46$) and predicted κ from SANS results yields values within 31 % of the experimental value at 25 mM.

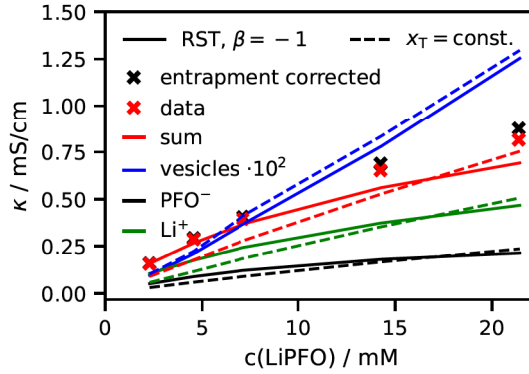


FIG. 4. Conductivity vs. concentration of LiPFO and samples with $\alpha_T = \frac{3}{7}$ at 25.0 °C. Lines indicate simulated contributions from vesicles, unimers or Li^+ counterions as well as their sum, which predicts values for the entrapment corrected data.

4. Scattering from Free Surfactant Molecules

For the question of the whereabouts of the remaining surfactant, i.e. to bridge the gap between sample and vesicle compositions, x-ray scattering is better suited than SANS as it is spared from the incoherent contributions. However, in general free surfactant molecules will contribute a q -dependent scattering distribution and for a precise analysis this has to be taken into consideration.

We fit a cylinder form factor to SAXS data of 12.5 mM PFO^- in solution. The resulting intensity can then be scaled to represent PFO^- unimers at different concentrations. The fit in log-log scale conserves scattering length of the individual molecules and the length of the perfluorinated chain (0.984 nm) by imposing a relationship between SLD, cylinder radius, and volume fraction (see SII C).

The fit result is shown in figure 5 and is used as background for further analysis of the SAXS data with a scaling factor according to the concentration of free LiPFO.

Cylindrical shapes have been used before to represent surfactant molecules in solution. Examples with varying degrees of abstraction can be found in the literature, e.g. as beads on a straight line²⁹, rigid rods³⁰, and infinitely thin rods³¹. Other approaches to scattering from individual small molecules would be, for example, the Debye function for a (very short) polymer coil³² or using the data to determine an empirical form factor³³. The cylinder was chosen here due to the clear q^{-1} power law.

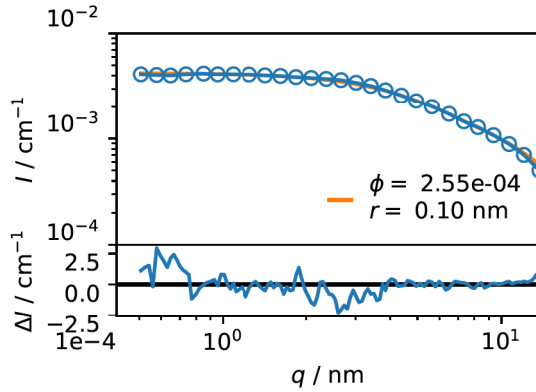


FIG. 5. Cylinder fit to a 12.5 mM solution of LiPFO in H_2O . For clarity, data was rebinned for plotting.

The free PFO^- contributes non-negligible coherent scattering especially in the region around the bilayer minimum (1.3 nm^{-1}) and the q^{-1} power law at high q . The expected intensity

lies between $2.53 \times 10^{-3} \text{ cm}^{-1}$ and $2.77 \times 10^{-3} \text{ cm}^{-1}$ for SAXS and $1.80 \times 10^{-4} \text{ cm}^{-1}$ and $1.97 \times 10^{-4} \text{ cm}^{-1}$ for SANS in D_2O . These values are compatible with the intensity at the bilayer minimum after background subtraction, $2.94 \times 10^{-3} \text{ cm}^{-1}$ in SAXS and $2 \times 10^{-3} \text{ cm}^{-1}$ in SANS. The upper limit for the concentration of free PFO^- compatible with SAXS data is hence about 8.6 mM, i.e. in good agreement with the previous estimates regarding the composition of the bilayer.

C. Structural properties: bilayer (a)symmetry

With the correct volume fraction, composition and background, the question of analyzing the structural properties of the SUVs can be addressed quantitatively, with the aim of deducing detailed information regarding the internal structure of the bilayers. Starting from the simplest approach for SAS modelling of vesicles—a hollow shell with constant SLD—we increased the complexity of the radial profile $\text{SLD}(r)$, i.e. the internal structure of the bilayer, step by step, using the systems' physical properties as guide and constraint.

1. *homogeneous shell*

Figure 6 shows a hollow shell model fitted to the data based on the results from section III B. In order to obtain a reliable value for the aggregate volume, we weigh the low q region most by fitting I vs. q up to just below the first minimum of the bilayer form factor, 1.3 nm^{-1} for SAXS and 2 nm^{-1} for SANS. Later refinement of the model employs $I \cdot q^2$ vs. q (Kratky plot, eq. 8) in order to weigh data similarly over the q -range used. We use a Schulz-Zimm distribution³⁴ (eq. 11) for the vesicle radius or volume and the scattering of the free PFO^- is accounted for by $I_{\text{cyl}}(q)$. Equation 9 gives the scattering intensity of a hollow shell with the form factor amplitude of a

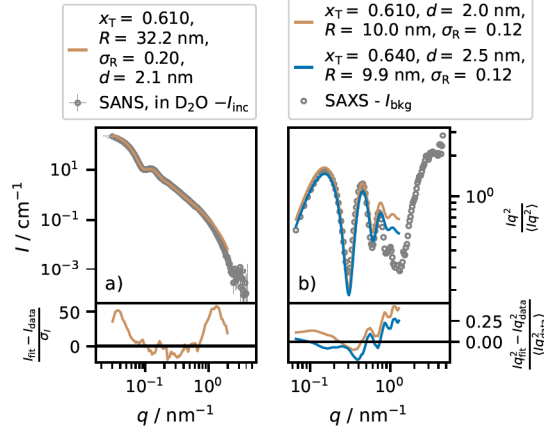


FIG. 6. a) Fit of a homogeneous shell form factor to the background-subtracted SANS data in D₂O (7 h to 15 h sample age). Aggregate composition (and hence SLD) is fixed, whereas ϕ_{ves} and aggregate dimensions (R, t) are optimized in $\log(I)$ vs. $\log(q)$. The resulting mean volume fraction is used for the SAXS fit of R, d (b), light brown, sample age 13.2 s). Results and residuals are shown in a Kratky plot ($I \cdot q^2$ vs. q) to clearly represent the entire q -range. For the SAXS data a second line (blue) shows the result of fitting the vesicle composition x_T , radius and thickness to I .

sphere of radius R , $k_{\text{Sph}}(R)$ (eq. 10).

$$I(q) \cdot q^2 = I_{\text{sh}}(q) \cdot q^2 + I_{\text{cyl}}(q) \cdot q^2 \quad (8)$$

$$I_{\text{sh}} = \frac{\phi}{V_{\text{sh}}} \int_{R_0-3\sigma}^{R_0+3\sigma} dR p_{\text{SZ}}(R, R_0, \sigma) \cdot ((\text{SLD}_{\text{solv}} - \text{SLD}_{\text{sh}}) k_{\text{Sph}}(R + d/2) + (\text{SLD}_{\text{sh}} - \text{SLD}_{\text{solv}}) k_{\text{Sph}}(R - d/2))^2 \quad (9)$$

$$k_{\text{Sph}}(R) = 4\pi \frac{\sin(q \cdot R) - q \cdot R \cdot \cos(q \cdot R)}{q^3} \quad (10)$$

$$p_{\text{SZ}}(x, x_0, \sigma) = \frac{z^z x^{z-1}}{e^{xz} x_0 \Gamma(z)}; z = \frac{1-p^2}{p^2}; p = \frac{\sigma}{x_0} \quad (11)$$

Here, R_0 and σ are mean and standard deviation of the radius R . The thickness of the shell is denoted d and SLD_{solv} and SLD_{sh} are the scattering length densities of the solvent and the shell, respectively.

With the composition of the SUVs $x_T = 0.61$ obtained from SANS the bilayer thickness in

SAXS is estimated as 2.0 nm (Fig. 6 b, light brown). This value is technically in agreement with the surfactant dimensions and corresponds to almost exactly twice the stretched length of LiPFO. However, it is clear from the data that the thickness must be higher, both the decrease at mid- q and the feature at 2.3 nm^{-1} point to higher values. We expect a difference in thickness between SANS and SAXS which is related to different SLD profiles for x-rays and neutrons: for SAXS, contrast is much higher for the shorter LiPFO, whereas the longer TDMAO contributes more in SANS. Accordingly, in SAXS the outside of the bilayer is weighted more, making it look thicker, in SANS, the inside is weighted more, making it look thinner.

On the other hand, the difference in radius observed between SAXS and SANS is expected from the kinetic evolution in the system¹⁴. This evolution underlines the fact that the system has not reached thermodynamic equilibrium at least during the SAXS measurement (13.2 s after mixing) and therefore some difference in mixing ratio x_T between SAXS and SANS is possible. Due to the strongly attractive interaction between both surfactants, a decrease of x_T towards equimolarity over time is more likely than a change in the opposite direction.

Mixing ratio x_T , radius and bilayer thickness were optimized against the data in I vs. q . As in SANS contrast variation, x_T was coupled to the concentration of PFO⁻ unimers (see SIII C). The best fit is shown in (Fig. 6 b, blue) with $x_T = 0.64$, this increases the concentration of PFO⁻ unimers from 7.4 mM (in contrast variation SANS) to 8.3 mM (in SAXS), both values compatible with the data and conductivity measurements. Hence, the mixing ratio x_T appears to decrease by 5 % between 13.2 s (SAXS) and 7 h to 15 h after mixing (SANS) due to incorporation of 0.8 mM LiPFO into the bilayer. While the finding that x_T during SANS and SAXS measurements differ by 5 % limits the comparability of both techniques, SANS contrast variation importantly provides evidence that x_T is significantly higher than RST would predict, and could thereby be used as a reasonable starting point and guide for SAXS analysis.

In terms of form factor parameters, the average scattering length density of the vesicle shell is $\text{SLD}_{\text{ves},x} = 0.00109 \text{ nm}^{-2}$ and $\text{SLD}_{\text{ves},n} = 0.00012 \text{ nm}^{-2}$ for x-rays and neutrons, respectively. The volume fraction of vesicles ϕ_{ves} is 0.0047 for SANS and 0.0043 for SAXS.

The unimer concentration of LiPFO is added as a background during the fit, while the incoherent background is subtracted as the minimum of the data in SANS. Regarding the aggregate dimensions that were allowed to vary, information on the vesicle radius is reliably available from the data, while we employ the surfactant dimensions to estimate boundaries on the thickness. Bilayer thickness must be smaller than twice the stretched length of TDMAO including its headgroup

($2 \times 2.19 \text{ nm}$). For the SAXS sample the intensity is more sensitive to the LiPFO content, but the bilayer thickness is less accessible from the data.

Detailed fit results are available in the supporting information, figure S17. For further modeling of the SAXS data we employ the resulting mean of the aggregate volume ($3.1 \times 10^3 \text{ nm}^3$) and polydispersity thereof (0.24) corresponding to Fig. 6 b.

Due to the near-perfect fit of the SANS data with the homogeneous shell form factor (Fig. 6 a) there was no need for another model. With the exception of the noisy dataset closest to the contrast match point, no systematic deviations from a homogeneous shell were found (see Fig. S10). Further structural analysis was therefore done on the SAXS data.

2. Vesicle Shell Profile

Description of our data using a homogeneous spherical shell is limited to the low- q region up to roughly $2\pi \cdot \text{thickness}^{-1}$. As we will show in this section, however, the effects of bilayer inhomogeneity are already relevant below this threshold.

As illustrated in figure 7, a layer containing only alkyl chains (part of the TDMAO tails) may occur in the bilayer center since TDMAO has much greater stretched length than LiPFO. For all bilayer thicknesses greater than twice the stretched length of LiPFO ($2l_{\text{LiPFO}} \approx 2.0 \text{ nm}$) we therefore expect an inhomogeneous SLD profile with a sandwich-like structure. The upper limit for the thickness is $2 \times 2.19 \text{ nm}$ as before.

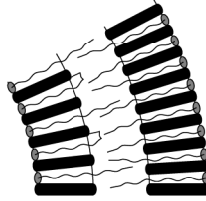


FIG. 7. Schematic representation of TDMAO (headgroup and thin tail) and LiPFO/PFO⁻ (black cylinders) in the vesicle.

Fig. 8 shows how the SLD profile is designed to correspond to a simplified molecular picture of the bilayer. For the alkyl chain region (shell 2), we use a SLD of 7.2 nm^{-2} (see VIC). For the mixed regions containing both perfluorinated and hydrocarbon surfactant (shells 1 and 3), contrast is fully determined by its average in the entire bilayer, the SLD of the alkyl chain shell,

and the dimensions of all regions. We introduce the symbol $3_{||}$ for this model with three shells and a symmetrical SLD profile (trivially, the homogeneous shell model becomes $1_{||}$ by analogy). The thickness of the mixed layers cannot exceed the length of the perfluorinated surfactant tail, 0.984 nm, plus the size of the headgroup region of about 0.3 nm. During optimization, the bilayer thickness was constrained to be larger than twice the thickness of the mixed layer. Similar models with step-like profiles have been used to describe vesicles in previous studies^{35–37}.

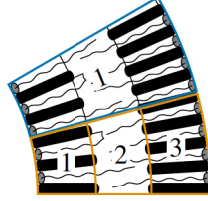


FIG. 8. Correspondence of SLD profile to a simplified molecular picture of the bilayer. Blue: homogeneous spherical shell model ($1_{||}$). Light orange: three-shell model $3_{||}$. Shells 1 and 3 facing the solvent contain a mixture of LiPFO and (parts of) TDMAO, whereas shell 2 contains TDMAO alkyl chains only.

As we enter subnanometer resolution, the scattering of the LiPFO unimers becomes relevant as well. This contribution was represented by a cylindrical form factor with dimensions according to section III B 4 and volume fraction fixed to correspond to 8.3 mM. In principle, the cylinder-like scattering of $\text{PFO}^-/\text{LiPFO}$ in the bilayer is also visible in the WAXS region, therefore the fit range of the core-shell model was limited to 2.5 nm^{-1} . Here and for all further fits, we use the aggregate volume fraction, vesicle composition/SLD and vesicle volume (including polydispersity) determined in sections III B and III C 1. By employing the vesicle volume as parameter, any small changes in bilayer thickness must be compensated by appropriate changes in the vesicle radius. We thereby prioritize the conservation of forward scattering intensity over a fixed radius.

Fit results are shown in figure 9. The three-shell model already captures the shape of the bilayer form factor, but underestimates intensity at mid- and high q , as seen in Fig. 9.

3. *Bilayer (A)symmetry*

We model asymmetry via the molar fraction of LiPFO in the outer shell, $x_{\text{LiPFO},0}$. The prior probability distribution of this parameters is derived from an estimate of the free enthalpy of mixing G_{mix} in the vesicle. In other words, we consider those values of $x_{\text{LiPFO},0}$ that minimize G_{mix}

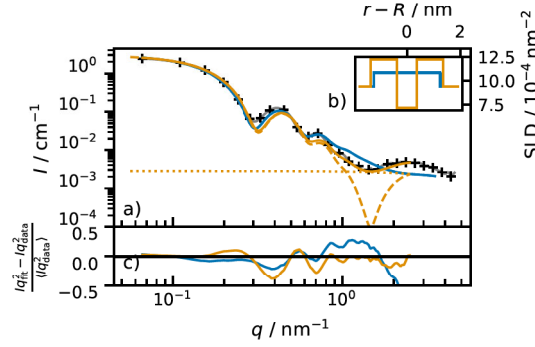


FIG. 9. Comparison of a symmetrical model containing three shells ($3_{||}$, orange) and a homogeneous spherical shell ($1_{||}$, blue). Bilayer thickness and the thickness of the mixed layer were allowed to change under the constraint that the $1_{||}$ model results be reproduced by averaging the three shells. a) Best fit and SAXS data. b) SLD profiles in the radial direction. c) Residuals in Iq^2 .

the most likely and set probability to zero for values that are unobtainable for a given vesicle composition x_{TDMAO} and geometry (R, t) . Specifically, we calculate the sum of ideal mixing free enthalpies for the inner and outer shell, $G \sim x \ln(x) + (1 - x) \ln(1 - x)$ respectively. As the mixing ratio of the entire bilayer is fixed, the mixing ratio of the inner layer is fully defined from the average, the value in the outer layer as well as the available headgroup area inside and outside. This estimate of G_{mix} is minimal for a symmetric bilayer with $x_{\text{LiPFO},o} = x_{\text{LiPFO}} = 1 - x_{\text{TDMAO}} \approx 0.36$, where x_{TDMAO} is the value obtained from SANS (see Fig. 3). The shape depends on the vesicle size. The prior probability density function (pdf) is then calculated according to $\text{pdf} = \exp(-\frac{G_{\text{mix}}}{RT})$ (Boltzmann factor), which leads to the distribution shown in figure 10. Details are described in the SI SV.

This prior probability distribution is used during the fit to draw values with higher probability with greater frequency. As before, we keep the vesicle volume and average SLD constant as well as the thickness of the mixed layers from the symmetrical fit $3_{||}$. The current model, three spherical shells allowing for an asymmetrical SLD profile, is designated 3_{\neq} .

Optimizing against SAXS data, the global best fit is at 40 %, this corresponds to an excess of LiPFO on the outside of 10 % with respect to a symmetrical bilayer.

Figure 11 shows the result together with the symmetrical profile from the previous section. Asymmetry improves the fit from the second local minimum on, reducing the slope of the intensity

decrease. This is plausible, as asymmetry reduces the effective thickness of the bilayer as seen by SAXS by "concentrating" the contrast in a smaller volume. The vesicle then appears closer to a flat bilayer with $I \propto q^{-2}$. However, intensity at the bilayer minimum is slightly overestimated. In this region we observe the largest influence of the PFO⁻ background, hence small errors of concentration or volume of those unimers may play a role here. We can also see clearly how the asymmetry significantly decreases the depth of the bilayer minimum as polydispersity of the bilayer thickness would as well. From the improvements at mid- q (second and third minimum) that asymmetry brings, however, we can be reasonably certain that polydispersity alone is not sufficient to describe the data.

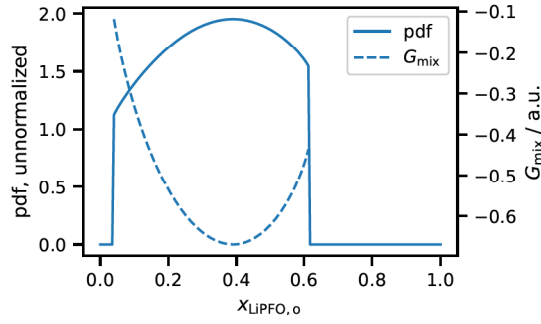


FIG. 10. Prior probability used in optimizing the mole fraction of LiPFO in the outer layer

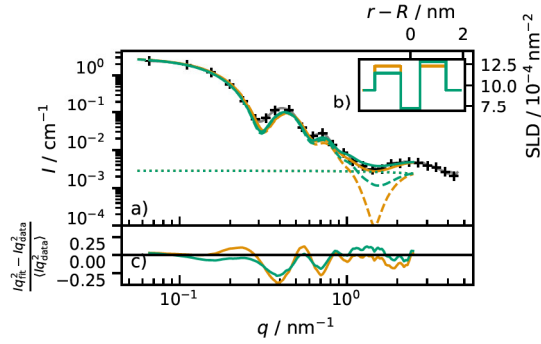


FIG. 11. Comparison of an asymmetrical model containing three shells ($3_{||}$, green) and a symmetrical model containing three shells ($3_{||}$, orange). The bilayer center is assumed to contain only alkyl chains. The shells facing the solvent are allowed to vary such that the total scattering length is conserved with respect to the 1-shell model. a) Best fit and SAXS data. b) SLD profiles in the radial direction. c) Residuals in Iq^2 .

4. 5-shell model

To include separate headgroup shells in our model, we introduce additional shells as shown in Fig. 12. We again begin calculation of the SLD profile from the average mixing ratio and SLD of the bilayer. The total vesicle volume is kept constant as before. In analogy to the previous models the model designation is 5_{\parallel} .

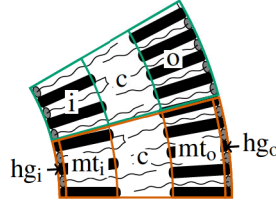


FIG. 12. Correspondence of SLD profile to a simplified molecular picture of the bilayer. Green: three-shell model 3_{\parallel} with inner (i), central (c) and outer (o) shell. Dark orange: five-shell model 5_{\parallel} . Shells i and o from before are divided into "mixed tails" (mt) and headgroup (hg) regions containing the respective parts of the surfactant molecules, whereas shell c is unchanged with respect to the three-shell model.

We use asymmetry and total bilayer thickness as fit parameters. Scattering lengths and volumes for the entire surfactant molecule and its tail^{38,39} are fixed. By confining the surfactant tails to the shells c, mt_i and mt_o (see Fig. 12) and using the stretched length of the perfluorinated surfactant, 0.984 nm, as the length of the "mixed tails" shells, the SLD of those shells depends on the average molar mixing ratio and asymmetry only. From these parameters, we derive the headgroup SLD and headgroup layer thickness such that volume and scattering length of both the surfactant molecules are conserved. The central shell again consists of hydrocarbon chains only and aggregate volume fraction ϕ , vesicle composition/SLD and vesicle volume (incl. polydispersity) remain fixed. Details of those calculations can be found in the supporting information SVIE. Optimization results are shown in figure 13. Optimization of LiPFO content in the outer layer and bilayer thickness yields 40 % and 2.8 nm, both parameters slightly larger than for the previous three-shell model. However, χ^2 also increases by about 11 % when using this heavily constrained five-shell model as compared to the previous three-shell model with asymmetric profile. Therefore, we abort the search for a better step-like profile at this point. Limitations of form factors with sharp changes in SLD are not surprising for surfactant aggregates in the liquid state. Here, we do not expect any sharp interfaces, and the increase in χ^2 confirms that the bilayer structure is not as constrained as

model 5_{\parallel} assumes.

We can expect the shell-based model to break down at high q as soon as individual molecules are resolved within the vesicle. Due to the high contrast between TDMAO and LiPFO chains and judging from the scattering of LiPFO unimers, a description using laterally homogeneous SLDs is expected to break down between 2 nm^{-1} and 3 nm^{-1} . Below this region in q we can now compare parameters and residuals for four SLD profiles.

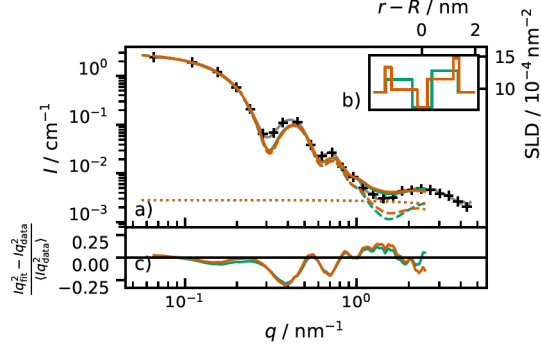


FIG. 13. Comparison of an asymmetrical profile with 5 shells (5_{\parallel} , dark orange) and an asymmetrical model containing three shells (3_{\parallel} , green). Parameters are given in Table II and SVIE; overall bilayer thickness and asymmetry of the LiPFO distribution were used as fit parameters. a) Best fit and SAXS data. b) SLD profiles in the radial direction. c) Residuals in Iq^2 .

5. Comparison

In Table II all fit parameters are summarized. As discussed before, all parameters except those in Table II were kept constant or derived from molecular properties of the constituents as discussed in the respective sections (for details see the SI). Figure 14 shows an overview of fit residuals. From low to high q , we first observe an improvement from a homogeneous to an inhomogeneous bilayer profile. A crossover is observed at about 0.3 nm^{-1} , the first local minimum. Thereafter, the asymmetric three- and five-shell models yield the best approximations to the data. With the exception of a small region around the second local minimum, the five-shell model does not improve the fit further. While the five-shell model comes with a different SLD profile, it does not increase the number of free parameters because many of its properties are determined by the molecular

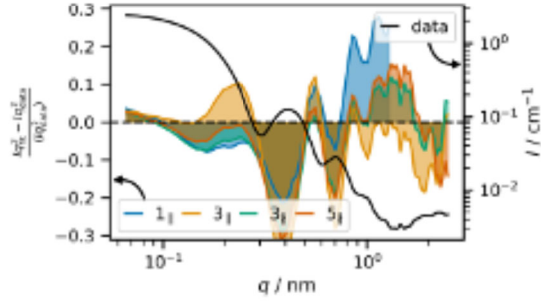


FIG. 14. Theory minus data in Kratky scale. Areas between residuals and zero are colored to better illustrate magnitude and sign of discrepancies in different q -ranges. Data is shown for reference.

structure of the two surfactants. Any further improvements would probably require profiles with continuous and smooth transitions between shells.

TABLE II. Parameters optimized for each model with best fit results. The model designations are <number of shells>_{||}(symmetrical)/_{||}(asymmetrical) SLD profile.

model	parameter	best unit
1	radius	9.9(18) nm
1	thickness	2.48(70) nm
1	x_surf1_vesicle	0.640(35)
1	c(PFO ⁻)	8.27 mM
3	thickness13	0.98(20) nm
3	thickness	2.71(27) nm
3	thickness	2.70(13) nm
3	x_surf2_3	0.397(54)
5	thickness	2.78(20) nm
5	x_surf2_o	0.401(47)

IV. DISCUSSION

The zwitterionic surfactant mixture TDMAO/LiPFO forms spontaneously small unilamellar vesicles (SUV), whose detailed bilayer structure was in the center of this work. This surfactant

mixture shows strong attractive interactions, characterized by a β value of $-12kT$, as calculated from cmc values determined by surface tension measurements. However, analyzing in thorough detail SAXS and SANS data at $c_{\text{tot}} = 25 \text{ mM}$ and $\alpha_T = \frac{3}{7}$ shows that a much higher fraction of the LiPFO must be present in the form of free molecules than predicted by Regular Solution Theory. The bilayer composition was directly determined by SANS contrast variation and the obtained value of $x_T = 0.61$ was corroborated by measurements of electrical conductivity and applicable to SAXS data on a recently mixed sample with a minor adjustment of 5 %. Since this adjustment or discrepancy between SANS and SAXS is rather small and in line with the expected trend towards equimolarity over time for strongly interacting surfactant pairs, results from SANS provide strong evidence to guide the analysis of the SAXS data—the marked deviation from RST results and their direction—even if the exact composition is not the same.

The deviation towards more aggregated TDMAO is consistent with the surfactants' cmcs and must be linked to the chemical potential of the surfactants in the bilayer. Accordingly, one can assume that this effect will similarly be present for other binary surfactant mixtures strongly asymmetric in their cmc values. Using the correspondingly corrected volume fraction and the bilayer composition then allowed for a reliable quantitative analysis of the SAXS and SANS data.

Using simple but constrained geometric models, we find an asymmetric SLD profile with more LiPFO in the outer layer and therefore a more negatively charged outer surface. This is plausible considering packing geometry as well as electrostatic considerations favoring similar ion concentrations inside and outside of the vesicles. LiPFO is known to form spherical micelles, while TDMAO tends to form rod-like micelles, a sign of a higher packing parameter. Hence, it may be easier to accommodate PFO^- into the layer with positive curvature.

Our empirical result of an asymmetric bilayer is supported by theories based on curvature considerations⁴⁰ and molecular packing theories^{41,42} confirm the intuition that the short-chain surfactant should be the one with an increased mole fraction in the outer layer. While quantitative calculation of the expected composition according to the theory by Yuet and Blankschtein⁴² for catanionics that considers, among other factors, chain conformation and packing is prohibitively complex, we can estimate packing parameters⁴³ and discuss the observed curvatures in our system. With the composition of inner and outer layer from our analysis, we can subdivide the hydrophobic portion of the vesicle shell volume ($d_{\text{hydrophobic}} = 2.27 \text{ nm}$) into two layers and calculate effective packing parameters for both based on the thicknesses of those layers. We obtain $p_{\text{eff},i} = 1.12$ and $p_{\text{eff},o} = 0.89$ ($a_{\text{hg},T} = a_{\text{hg},L} = 0.32 \text{ nm}^2$). Using a linear combination of curvatures as a simple

approximation⁴⁴, we can estimate the effective curvatures of both surfactants individually in the outer layer of the vesicle. The results are $c_{o,T} = 0.05 \text{ nm}^{-1}$ and $c_{o,L} = 0.16 \text{ nm}^{-1}$, assuming both curvatures decrease by the same percentage (83 %) compared to the individual micelles due to the attractive interactions.

Thus, an asymmetric bilayer with more LiPFO in the outer layer is plausible in terms of curvature, since creating the inner layer with negative curvature will be even more unfavourable for LiPFO.

Interestingly, the dimensions of the vesicle expressed in the quantities used by Yuet and Blankschtein⁴², dimensionless curvature of the hydrophobic domain \bar{c} and fraction of molecules in the outer layer f , lie close to a local minimum of the vesicle Gibbs energy which they find at $\bar{c} = 0.2$ with $f \approx 0.6$ for a C_{16}/C_8 catanionic system at $x_{C_{16}} = 0.5$. This local minimum becomes less pronounced and shifts to slightly higher \bar{c} if the chain length difference is decreased⁴⁵. In our case (C_{14}/C_8 system), we have $\bar{c} = 0.18$ and $f = 0.613$, hence packing may play an important role here and be related to the small polydispersity of the aggregates.

It should be noted that a marked asymmetry of the bilayer composition of mixed surfactant vesicles has been reported a long time ago for the system TX100/octanol/CPCl and could be explained on the basis of an electrostatic model⁴⁶. This model accounts also for the entropy of the counterions and the bilayer and from minimizing the free energy yields the size of the formed vesicles as well as the extent of asymmetry of the bilayer composition.

These findings complement the discussion of catanionics above since TDMAO is not permanently charged. Electrostatic effects and counterion confinement are expected to play a role, since the inner radius of the vesicle, 8.55 nm, is only roughly three times the bulk Debye length in the system. Such confinement of counterions, let alone unimers, is thermodynamically unfavorable. Hence, the chemical potential of LiPFO in the vesicle should be enhanced and therefore automatically result in a higher LiPFO unimer concentration in the bulk and a higher LiPFO mole fraction in the outer layer.

From the increased LiPFO unimer concentration it can be concluded that its chemical potential in the aggregates is increased as compared to RST predictions. The magnitude of this effect appears to decrease over time (SAXS vs. SANS measurements), while the radius of the vesicles increases. Thus, there is reason to believe the deviation from RST is, at least in part, related to the presence and size of SUVs which determine the local chemical potential of LiPFO. The vesicles studied here are presumably not in a real thermodynamic equilibrium but in a long-lived metastable

state, that has a correspondingly higher chemical potential than that assumed in applying RST.

As an important outcome it can be stated that a careful and comprehensive analysis of scattering data of vesicles composed of mixed surfactants requires precise knowledge of the bilayer composition, which can deviate largely from that of the total bulk system. This can be done by contrast variation, provided sufficient contrast can be achieved between the surfactant components. Armed with this information one is then able to deduce quantitative information regarding the asymmetric distribution of the different surfactants within the bilayer, which is essential information for understanding their stability and properties. This approach is generally applicable and therefore can be applied rather generally for gaining a deeper understanding of vesicular systems with respect to their detailed structure and the mechanism of stabilisation of these structures.

V. SUPPLEMENTARY MATERIAL

Supplementary material provides further detail on the analysis of SAXS, SANS and conductivity data. It includes the derivation of the prior probability employed for the mole fraction of LiPFO in the outer layer and one graph showing the predictions of RST for a range of β and c_{tot} . Furthermore, results of the Markov-chain Monte Carlo optimization are shown and discussed.

VI. ACKNOWLEDGEMENTS

A.F.H. acknowledges funding by the BMBF (Grant No. 05K16KT1) and thanks the ESRF for the one-month traineeship which initiated this work and synchrotron beamtime as well as Dr. S. Prévost for helpful discussions. This work is based upon experiments performed at the KWS-1 instrument operated by JCNS at the Heinz Maier-Leibnitz Zentrum (MLZ), Garching, Germany. This work benefited from the use of the SasView application, originally developed under NSF award DMR-0520547. SasView contains code developed with funding from the European Union's Horizon 2020 research and innovation programme under the SINE2020 project, grant agreement No 654000.

VII. AUTHOR DECLARATIONS

A. Conflict of Interest

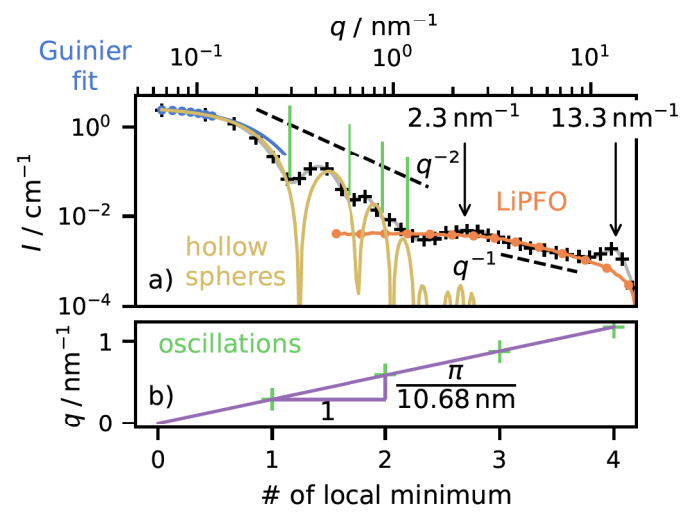
The authors have no conflicts to disclose.

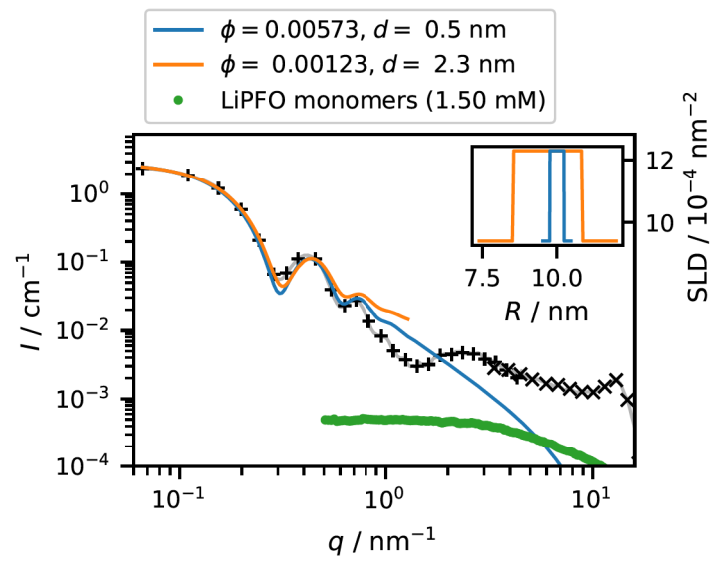
REFERENCES

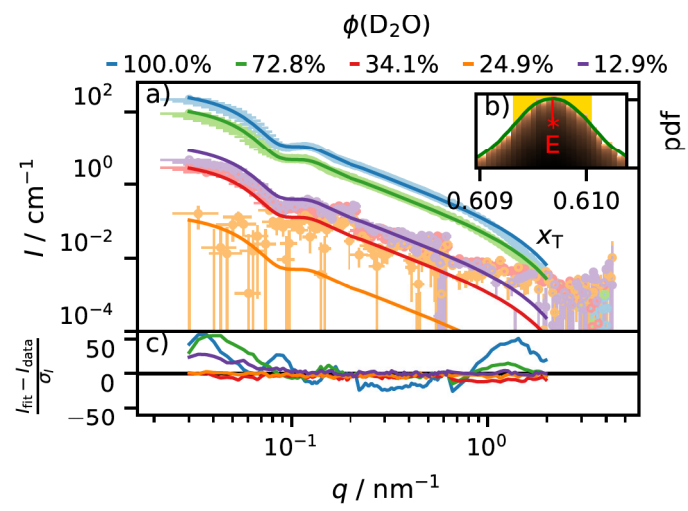
- ¹M. Gradzielski. *Journal of Physics: Condensed Matter* 15, 655 (2003).
- ²S. Šegota and D. U. I. Težak. *Advances in Colloid and Interface Science* 121(1-3), 51 (2006).
- ³E. Soussan, S. Cassel, M. Blanzat, and I. Rico-Lattes. *Angewandte Chemie International Edition* 48(2), 274 (2009).
- ⁴P. Fromherz and D. Ruppel. *FEBS Letters* 179(1), 155 (1985).
- ⁵P. Fromherz. *Chemical Physics Letters* 94(3), 259–266 (1983).
- ⁶Y. Xia, I. Goldmints, P. W. Johnson, T. A. Hatton, and A. Bose. *Langmuir* 18(10), 3822 (2002).
- ⁷A. Shioi and T. A. Hatton. *Langmuir* 18(20), 7341 (2002).
- ⁸J. Leng, S. Egelhaaf, and M. Cates. *Biophysical Journal* 85(3), 1624 (2003).
- ⁹W. Helfrich. *Physics Letters A* 50(2), 115 (1974).
- ¹⁰C. Wolf, K. Bressel, M. Drechsler, and M. Gradzielski. *Langmuir* 25(19), 11358 (2009).
- ¹¹T. M. Weiss, T. Narayanan, C. Wolf, M. Gradzielski, P. Panine, S. Finet, and W. I. Helsby. *Phys. Rev. Lett.* 94, 038303 (2005).
- ¹²T. M. Weiss, T. Narayanan, and M. Gradzielski. *Langmuir* 24(8), 3759 (2008).
- ¹³S. J. Burkitt, R. H. Ottewill, J. B. Hayter, and B. T. Ingram. *Colloid and Polymer Science* 265(7), 628 (1987).
- ¹⁴J. Gummel, M. Sztucki, T. Narayanan, and M. Gradzielski. *Soft Matter* 7(12), 5731 (2011).
- ¹⁵K. Bressel, S. Prévost, M.-S. Appavou, B. Tiersch, J. Koetz, and M. Gradzielski. *Soft Matter* 7(23), 11232 (2011).
- ¹⁶K. Bressel, M. Muthig, S. Prévost, J. Gummel, T. Narayanan, and M. Gradzielski. *ACS Nano* 6(7), 5858 (2012).
- ¹⁷K. Bressel. *Controlling Vesicle Systems by Amphiphilic Copolymers*. Ph.D. thesis, Technische Universität Berlin (2013).
- ¹⁸T. Narayanan, J. Gummel, and M. Gradzielski. volume 20 of *Advances in Planar Lipid Bilayers and Liposomes*, 171 – 196. Academic Press (2014).

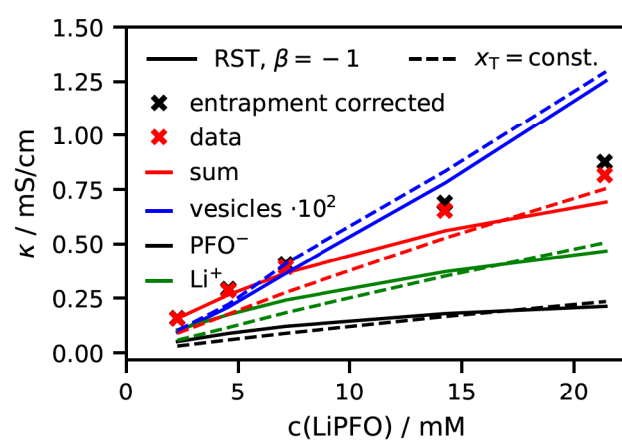
- ¹⁹V. Pipich. <https://www.qtisas.com/qtikws> (2017).
- ²⁰D. N. Rubingh. *Mixed Micelle Solutions*, 337–354. Springer New York, Boston, MA (1979).
- ²¹P. M. Holland and D. N. Rubingh. *The Journal of Physical Chemistry* 87(11), 1984 (1983).
- ²²I. Grillo, J. Penfold, I. Tucker, and F. Cousin. *Langmuir* 25(7), 3932 (2008).
- ²³I. Grillo and J. Penfold. *Langmuir* 27(12), 7453 (2011).
- ²⁴J. A. Vrugt, C. ter Braak, C. Diks, B. A. Robinson, J. M. Hyman, and D. Higdon. *International Journal of Nonlinear Sciences and Numerical Simulation* 10(3), 273 (2009).
- ²⁵P. Kienzle, J. Krycka, N. Patel, and I. Sahin. College Park, MD: University of Maryland (2011).
- ²⁶A. F. Hörmann. <https://gitlab.com/ahoermann/tdmao-lipfo-high-monomer-concentration-asymmetric-bilayer.git> (2023).
- ²⁷P. Gianni, L. Bernazzani, C. A. Guido, and V. Mollica. *Thermochimica Acta* 451(1-2), 73 (2006).
- ²⁸G. S. Manning. *The Journal of Physical Chemistry B* 111(29), 8554 (2007).
- ²⁹G. V. Jensen, R. Lund, J. Gummel, M. Monkenbusch, T. Narayanan, and J. S. Pedersen. *Journal of the American Chemical Society* 135(19), 7214 (2013).
- ³⁰M. J. Hollamby, K. Trickett, A. Mohamed, J. Eastoe, S. E. Rogers, and R. K. Heenan. *Langmuir* 25(22), 12909 (2009).
- ³¹L. M. Bergström, S. Skoglund, K. Edwards, J. Eriksson, and I. Grillo. *Langmuir* 29(38), 11834 (2013).
- ³²L. Arleth and J. S. Pedersen. *Journal of Applied Crystallography* 33(3), 650 (2000).
- ³³A. E. Harrak, G. Carrot, J. Oberdisse, J. Jestin, and F. Boué. *Polymer* 46(4), 1095 (2005).
- ³⁴B. H. Zimm. *The Journal of Chemical Physics* 16(12), 1099 (1948).
- ³⁵J. A. Bouwstra, G. S. Gooris, W. Bras, and H. Talsma. *Chemistry and Physics of Lipids* 64, 83 (1993).
- ³⁶S. Ristori, J. Oberdisse, I. Grillo, A. Donati, and O. Spalla. *Biophysical Journal* 88(1), 535 (2005).
- ³⁷B. Eicher, F. A. Heberle, D. Marquardt, G. N. Rechberger, J. Katsaras, and G. Pabst. *Journal of Applied Crystallography* 50(2), 419 (2017).
- ³⁸V. Srinivasan and D. Blankschtein. *Langmuir* 21, 1647 (2005).
- ³⁹C. Tanford. *Journal of Physical Chemistry* 76(21), 3020 (1972).
- ⁴⁰S. A. Safran, P. Pincus, and D. Andelman. *Science* 248(4953), 354 (1990).

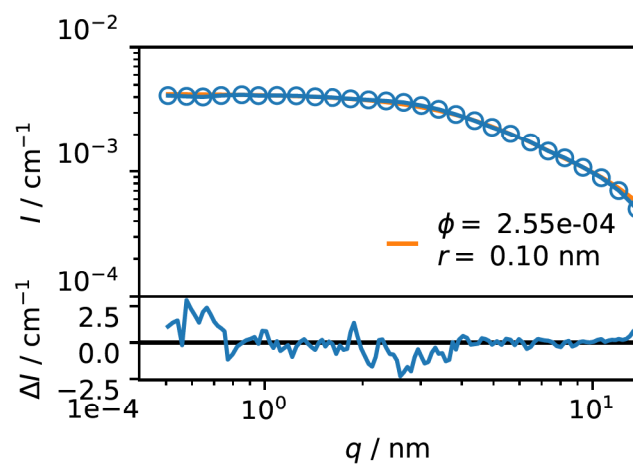
- ⁴¹J. N. Israelachvili, D. Mitchell, and B. W. Ninham. *Biochimica et Biophysica Acta (BBA) - Biomembranes* 470(2), 185 (1977).
- ⁴²P. K. Yuet and D. Blankschtein. *Langmuir* 12(16), 3802 (1996).
- ⁴³J. N. Israelachvili, D. J. Mitchell, and B. W. Ninham. *J. Chem. Soc., Faraday Trans. 2* 72, 1525 (1976).
- ⁴⁴H. Wennerström and D. M. Anderson. *Difference Versus Gaussian Curvature Energies; Monolayer Versus Bilayer Curvature Energies; Applications to Vesicle Stability*, 137–152. *Statistical Thermodynamics and Differential Geometry of Microstructured Materials*. Springer New York (1993).
- ⁴⁵P. K. Yuet and D. Blankschtein. *Langmuir* 12(16), 3819 (1996).
- ⁴⁶J. Oberdisse and G. Porte. *Phys. Rev. E* 56, 1965 (1997).

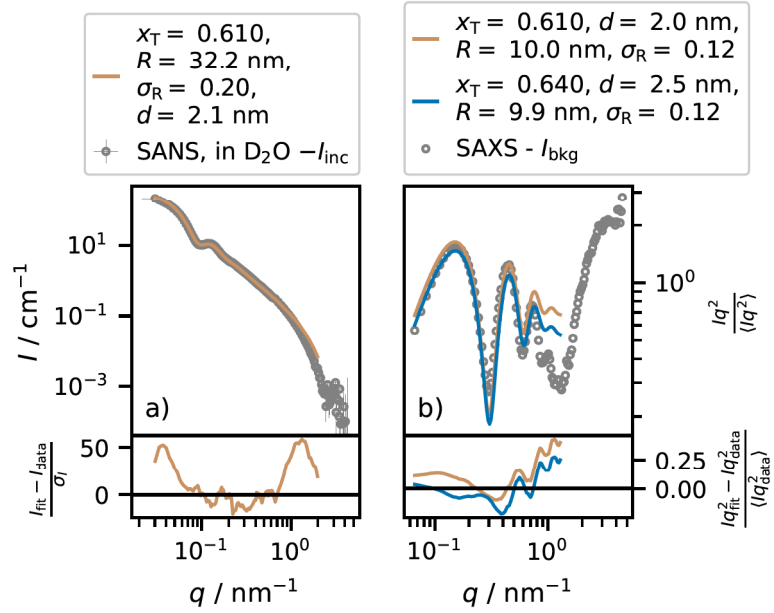






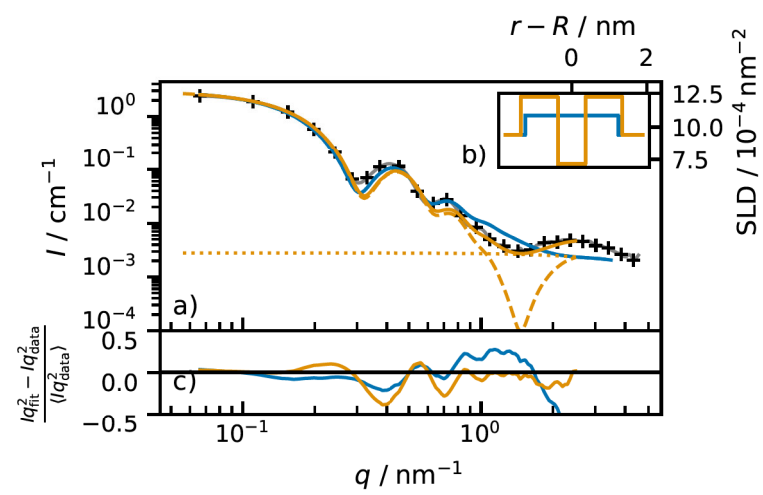


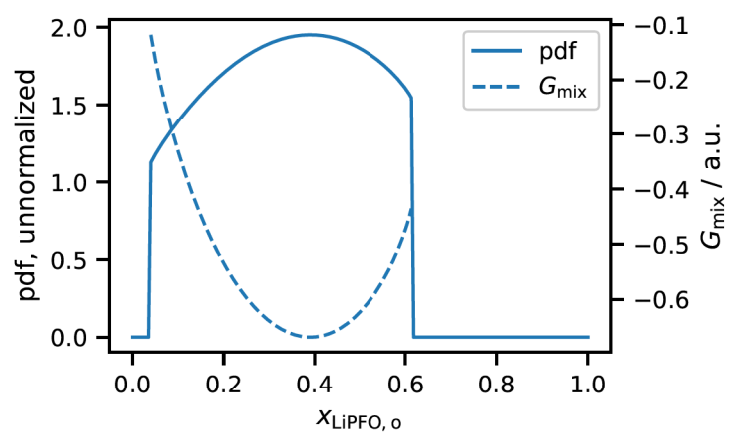


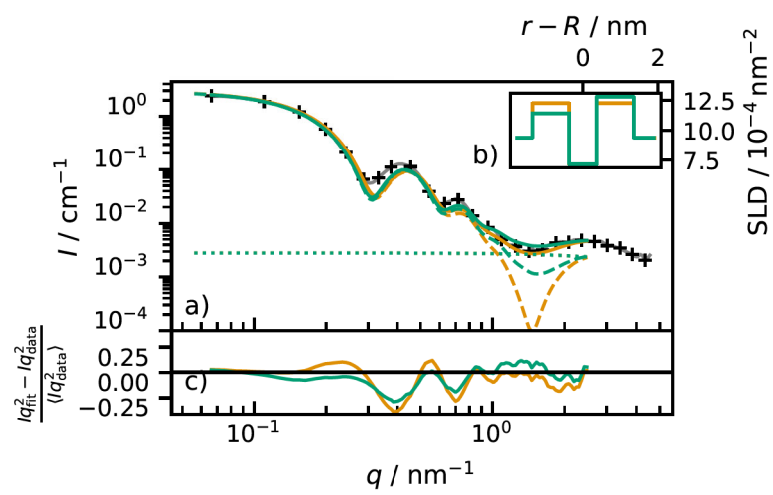












Accepted to J.
Chem. Phys.
10.1063/1.5002223

